Journal of Solid State Chemistry 182 (2009) 2829–2834

Contents lists available at ScienceDirect

Journal of Solid State Chemistry

journal homepage: www.elsevier.com/locate/jssc

Flash microwave synthesis and sintering of nanosized $La_{0.75}Sr_{0.25}Cr_{0.93}Ru_{0.07}O_{3-\delta}$ for fuel cell application

L. Combemale *, G. Caboche, D. Stuerga

Institut Carnot de Bourgogne, UMR 5209 CNRS-Université de Bourgogne, 9 Av. A. Savary, BP 47 870, F-21078 DIJON Cedex, France

ARTICLE INFO

Article history:
Received 6 May 2009
Received in revised form
18 July 2009
Accepted 22 July 2009
Available online 30 July 2009

Keywords:
Nanoparticles
Chemical synthesis
Perovskite
Solid oxide fuel cell (SOFC)
Microwave heating

ABSTRACT

Perovskite-oxide nanocrystals of $La_{0.75}Sr_{0.25}Cr_{0.93}Ru_{0.07}O_{3-\delta}$ with a mean size around 10 nm were prepared by microwave flash synthesis. This reaction was performed in alcoholic solution using metallic salts, sodium ethoxide and microwave autoclave. The obtained powder was characterised after purification by energy dispersive X-ray analysis (EDX), X-ray powder diffraction (XRD), BET adsorption technique, photon correlation spectroscopy (PCS) and transmission electron microscopy (TEM). The results show that integrated perovskite-type phase and uniform particle size were obtained in the microwave treated samples. At last the synthesised powder was directly used in a sintering process. A porous solid, in accordance with the expected applications, was then obtained at low sintering temperature (1000 °C) without use of pore forming agent.

1. Introduction

Perovskite-type oxide materials and their solid solution are used as electrode materials for solid oxide fuel cells (SOFCs) [1,2]. According to their mixed conductivity these materials exhibit two important functions, such as charge transport through both ions and electrons and efficient charge transfer at the oxygen/electrode interface.

$LaCrO_3$ is well known in SOFC system for interconnects materials because of its high melting point, relatively large electronic conductivity, low ionic conductivity and high chemical stability in both reducing and oxidising atmosphere [3,4]. The doping of a lower valence ion as Sr in La site increases the ionic conductivity, adjusts the thermal expansion coefficient with zirconia [5], eliminates the phase transition [6,7] and gives a low catalytic activity for the reforming reaction of hydrocarbon gas into hydrogen [8]. To enhance this latter property a chromium substitution by ruthenium was realised. Indeed it was proved that Ru makes a real positive contribution to catalytic activation for the reforming reaction [9,10].

According to Sauvet et al. [11,12] $La_{0.75}Sr_{0.25}Cr_{0.93}Ru_{0.07}O_{3-\delta}$ (noted LSCrRu) permits the use of hydrocarbon gas at the anode side in replacement of pure hydrogen. This process, called internal reforming, allows a good heat exchange between the endothermic reforming reaction and the exothermic electrochemical reaction within the stack (reaction (A)). Moreover the doped chromite lanthanum is resistant to the coking reaction (reaction (B)) the main problem reported for the use of the common anodic material Ni/YSZ with hydrocarbon gas [13].

$$H_2+O^{2-} \rightleftharpoons H_2O+2e^- \quad (A)$$

$$CH_4 \rightleftharpoons C+2H_2 \quad (B)$$

LSCr and LSCrRu perovskites are currently produced by spray pyrolysis technique [14], co-precipitation [15], solid state reaction [16] or citrate method [17]. These operating conditions are generally long time processes which give micrometric powder. Furthermore in LSCrRu case most of these techniques not ensure ruthenium integration in the perovskite structure. It could conduct to the lost of ruthenium, under RuO_3 or RuO_4 form, during the high temperature sintering process [18]. To prevent these problems microwave technology was employed.

Microwave heating is an emerging technology which uses the ability of liquids and solids to convert electromagnetic energy into heat. The specificities and the interests of microwave process are (i) heating rates induced close to several degrees per second, (ii) core heating and (iii) energy utilisation efficiency which can reach 80–90% [19–21]. These properties induce a particles nucleation in all volume by avoiding thermal parietal transfer. Therefore by monitoring time and temperature of the microwave treatment the particle growing is controlled and the synthesised powders present nanoparticles with a narrow size distribution. To raise kinetic reaction, microwave heating is performed with our

* Corresponding author. Fax: +33 3 80 39 61 32.
E-mail address: lionel.combemale@u-bourgogne.fr (L. Combemale).

0022-4596/$ - see front matter © 2009 Elsevier Inc. All rights reserved.
doi:10.1016/j.jssc.2009.07.040

original microwave autoclave reactor, the RAMO system (French acronym of Réacteur Autoclave Micro-Onde [22]). This laboratory device allows preparation of several kinds of nanomaterials as iron oxides [23], zirconia [24,25], titanium oxide [26], nanocomposites [27] and manganese oxide [28].

This work presents the first attempt to adapt and improve the microwave one-step flash synthesis for the production of $La_{0.75}Sr_{0.25}Cr_{0.93}Ru_{0.07}O_{3-\delta}$ under nanometric size. Nanoparticles were expected to decrease sintering temperature [27,28] and prevent reaction between anode, sintering support and electrolyte during a co-sintering process. According to Roosmalen et al. [29] a sintering temperature lower than 1000 °C prevents formation of parasite phases ($La_2Zr_2O_7$ and $SrZrO_3$) at electrode/electrolyte interface.

2. Experimental

2.1. Powder synthesis

All the starting materials, lanthanum nitrate hexahydrate (LaN_3O_9,6H_2O, Acros Organics, purity > 98%), strontium chloride hexahydrate ($SrCl_2$,6H_2O, Merck, purity > 98%), chromium nitrate nonahydrate (CrN_3O_9,9H_2O, Acros Organics, purity > 99%), ruthenium chloride ($RuCl_3$, Acros Organics, purity > 99%), sodium ethoxide (EtONa, Aldrich, 96%) and ethanol (Prolabo, Normapur, 96%) were used without further purification. Ethanol and sodium ethoxide, the associated base, were employed to achieve concomitant olation and oxolation reactions [28].

The general flowchart of the operating conditions was described previously [24]. Herein solution 1 was prepared by dissolving desired amounts of the selected salts in ethanol. The concentrations are fixed at 0.14 M for lanthanum, 0.06 M for strontium, 0.19 M for chromium and 0.02 M for ruthenium. Solution 2 was composed of sodium ethoxide 1 M in ethanol. These concentrations are chosen in order (i) to obtain a solid with a specific formula $La_{0.75}Sr_{0.25}Cr_{0.93}Ru_{0.07}O_{3-\delta}$, (ii) to allow complete dissolution of strontium chloride hexahydrate in ethanol (sol. max. = 0.142 M in ethanol [30]) and (iii) to product amount of powder as high as it possible. Solutions 1 and 2 were mixed and stirred in the RAMO system whereas a precipitate appears. The reactor was quickly sealed and an argon pressure was introduced (0.4 MPa). The treatments were decomposed into two steps. During the first step, the microwave power (1 kW) is applied until the pressure reaches a threshold value of 13×10^5 Pa with a heating rate equal to 10 °C s^{-1}. The selected pressure corresponds to a temperature close to 160 °C. During the second step, the pressure threshold is kept by monitoring the microwave power. This second step was carried out for 2 min to realise complete reaction and decrease agglomeration state.

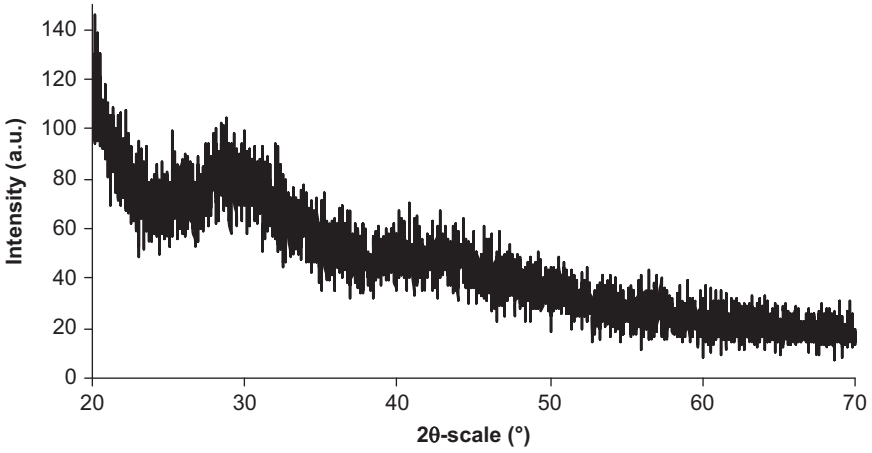

Fig. 1. X-ray pattern of LSCrRu raw powder.

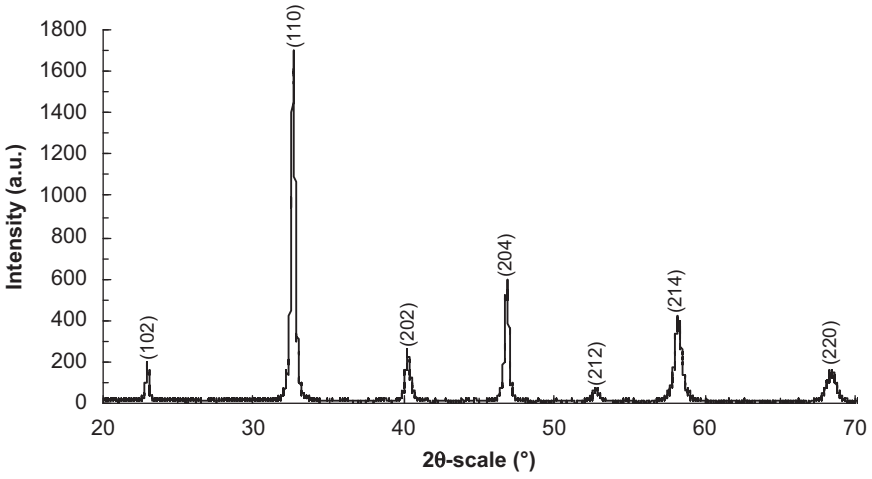

Fig. 2. X-ray pattern of LSCrRu powder after calcination at 1000 °C under argon.

Typically, 100 mg of nanosized $La_{0.75}Sr_{0.25}Cr_{0.93}Ru_{0.07}O_{3-\delta}$ was obtained in one step. The general balance of the reactional scheme is given by reaction (C):

$$0.75La(NO_3)_3 + 0.25SrCl_2 + 0.93Cr(NO_3)_3 + 0.07RuCl_3 + 5.75NaOEt + 5.75/2H_2O \rightarrow La_{0.75}Sr_{0.25}Cr_{0.93}Ru_{0.07}O_{3-\delta} + 5.04NaNO_3 + 0.71NaCl + 5.75EtOH \text{ (with } \delta = 0.125\text{)}.$$

Table 1
Elemental compositions (at%) for LSCrRu in initial mixture, after microwave synthesis and after calcination at 1000 °C under Ar atmosphere.

Element (at%)	La	Sr	Cr	Ru
Initial mixture	35±0.3	15±0.3	46.5±0.3	3.5±0.3
Microwave synthesised powder	37.6±0.6	12.4±0.9	47.2±0.4	2.8±0.2
Calcinated powder	37.4±0.3	12.6±0.7	46.2±0.2	3.8±0.1

After synthesis, purifications in distilled water were realised to remove NaCl and $NaNO_3$ formed during the microwave treatment. Na^+, Cl^- and NO_3^- species were provided by the different reagents. Finally, the powder was dried by cryogenic desorption to ensure the departure of water and prevent agglomeration.

2.2. Characterisation

The powder was studied after synthesis and after annealing treatments by different techniques. X-ray powder diffraction (XRD) patterns of the samples were recorded using a SIEMENS D-5000 diffractometer with Cu$K\alpha$ radiation source for phase identification. Raw powder morphology was defined by coupling different techniques: specific surface area was obtained by BET

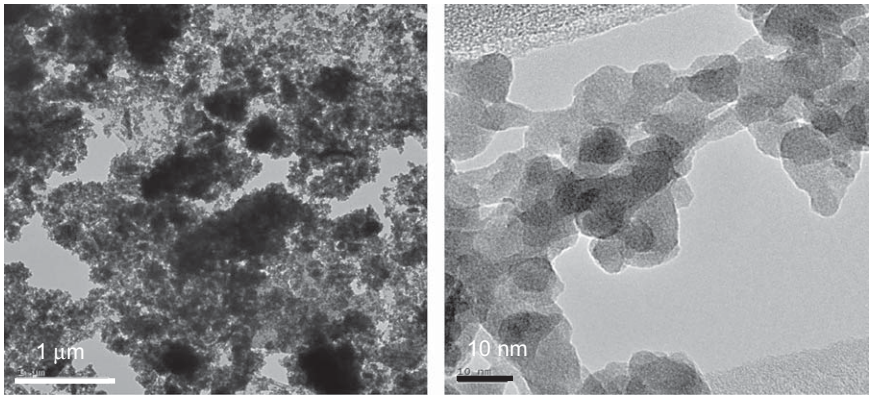

Fig. 3. TEM images from the raw LSCrRu powder.

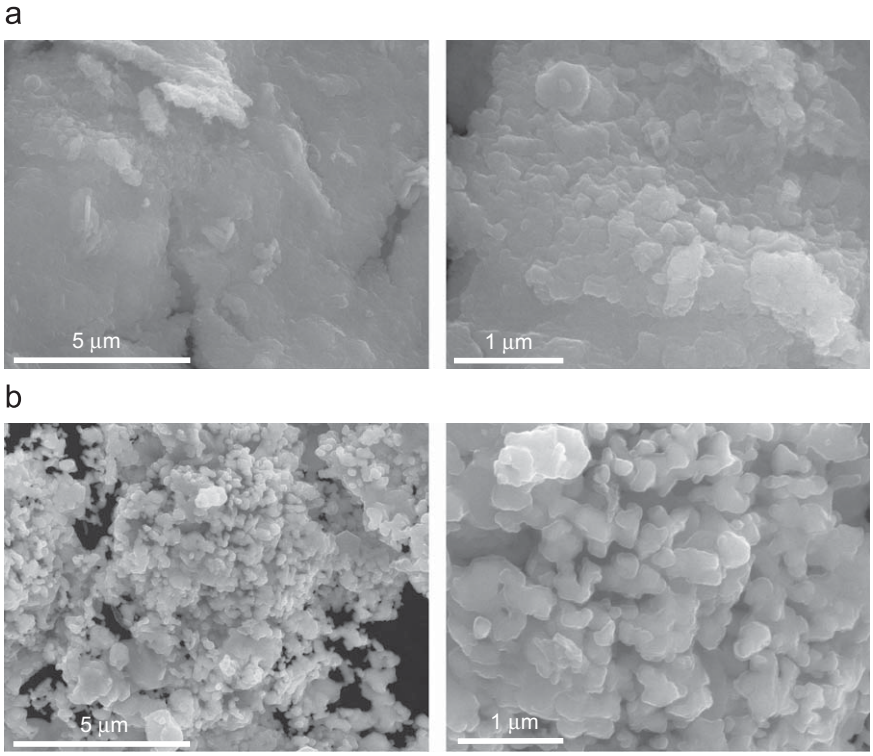

Fig. 4. Scanning electron microscopy micrographs from the raw (a) and the calcinated (b) powders.

with nitrogen at 77 K as adsorption gas (Autosorb 1 QUANTACHROME), particles size and morphology were observed by transmission electron microscopy (JEOL 2010 F) and the results were corroborate using photon correlation spectroscopy (7032 MALVERN Instruments). Finally chemical analysis was done on powders by using OXFORD INSTRUMENT—INCA ENERGY microprobe analyser and pure Cobalt as standard material. To realise X-ray spectra the LSCrRu powder was pressed into pellet form before analysis.

2.3. Sintering process

Pellets (20 mm diameter) were obtained by introducing raw powder in a working mould specially designed by authors. After uniaxial pressing the result was treated in a classic oven (AET Technology). A heating rate of 120 °C h^{-1} was applied and the holding time at the sintering temperature was 10 h. Sintering was carried out in an Ar atmosphere. The sintered pellets were then observed by scanning electron microscopy (JEOL JSM 6400F) to evaluate internal porosity. Density rate was determined using volume/mass ratio.

3. Results and discussion

3.1. Powder characterisation

Microwave treatment leads to the formation of LSCrRu powder. Fig. 1 presents a typical XRD pattern recorded for the as-synthesised powder. The diffraction pattern shows broad peaks due to the nanometric size and amorphous state of synthesised particles. To increase the crystallite size and improve crystalline state the powder was calcinated after microwave treatment. This step was realised in a classic oven at 1000 °C under low pressure of oxygen to prevent the formation of undesirable phases $LaCrO_3$ and $SrCrO_4$ as observed for $La_{1-x}Sr_xO_{3-\delta}$ (reaction (C) [31]).

$$La_{1-x}Sr_xCrO_3+(x/2)O_{2(g)} \Leftrightarrow (1-x)LaCrO_3+xSrCrO_4 \quad (C)$$

Fig. 2 presents XRD pattern obtained with calcinated powder. The peaks are thinner and correspond to LSCrRu materials. No ICDD card is available then the comparison was made with publication [14]. It confirms the formation of pure LSCrRu material. The parameter cell can be calculated with CELREF programme [32]. Considering LSCrRu as hexagonal phase R-3c the average value is estimated: $a = 5.51 \pm 0.01$ and $c = 13.34 \pm 0.01$ Å. Then the unit cell volume is determinate $V = 350.69$ Å^3. LSCrRu density ($d = 6.52$ g cm^{-3}) is deducted from the unit cell volume.

Further to the annealing heat treatment at 1000 °C a microprobe analysis is done to ensure ruthenium integration in the perovskite structure. This property can prevent formation of RuO_3 and/or RuO_4 which are unstable and volatile gases at high temperature [33,34]. Table 1 reports microprobe chemical analysis after microwave synthesis and after calcination at 1000 °C under Ar atmosphere. They are compared with initial mixture composition. The constant atomic concentration for ruthenium highlights the perfect integration of this element into the perovskite structure. A slight disappearance of strontium is observed after microwave treatment due to the low solubility of $SrCl_2$, $6H_2O$ in ethanol. This atomic loss lead to the formation of the desire composition: $La_{0.75}Sr_{0.25}Cr_{0.93}Ru_{0.07}O_{3-\delta}$.

The specific surface area is determined by applying the Brunauer–Emmet–Teller (BET) model to the microwave synthesised powder. A relatively high value of 100 $m^2 g^{-1}$ is then obtained. Assuming spheroids particles and only one layer of adsorbed nitrogen, a mean value diameter close to 10 nm can be calculated using density value.

The transmission electron microscope images are taken in order to estimate the size and show the morphology of the LSCrRu particles. Fig. 3 shows micrographies of the $La_{0.75}Sr_{0.25}Cr_{0.93}Ru_{0.07}O_{3-\delta}$ sample obtained after synthesis. Most of particles are spherical shaped crystals with an average size of 10 nm and present a low crystallisation state in accordance with the XRD patterns. In addition TEM images show formation of clusters due to the high surface energy. To observe the impact of thermal treatment on LSCrRu calcinated powder scanning electron microscopy images are provided (Fig. 4). They show submicrometric particles well-defined in calcinated powder case.

Fig. 5 displays the size distribution of LSCrRu nanopowder obtained by photon correlation spectroscopy (PCS) after ultrasonic treatment (10 min). The diagram represents the number repartition as a function of the particle diameter. Nanoparticle

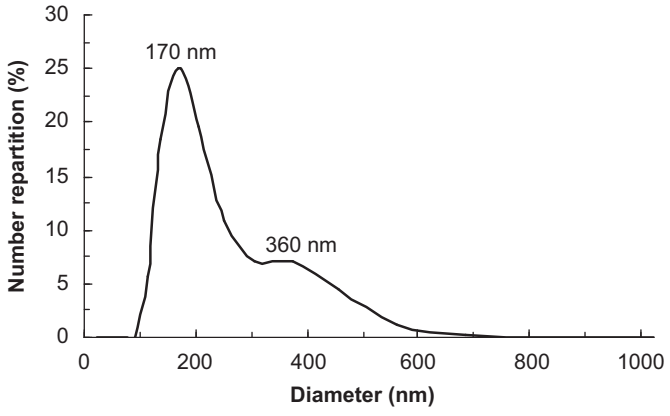

Fig. 5. Size distribution, obtained by PCS, of LSCrRu particles dispersed in distilled water after ultrasonic treatment.

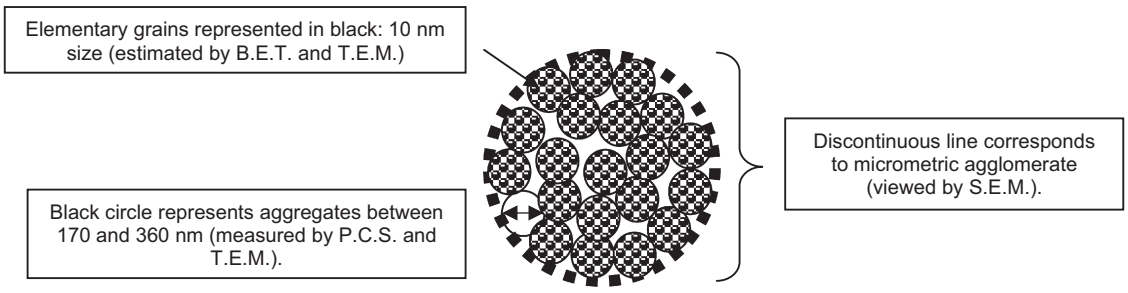

Fig. 6. Morphological model for LSCrRu powder synthesised using microwave technique.

size distribution shows different agglomeration degrees. This bimodal repartition is centred at 170 and 360 nm. Largest particles (360 nm) are association of two smallest elements (170 nm). Increasing the ultrasonic time treatment will give monomodal distribution centred at 170 nm. Nevertheless, no particles with nanometric size (10 nm diameter) are observed. It proves the high agglomeration state of the smaller elements.

All these observations lead to a morphological model presented in Fig. 6: elementary grains (10 nm) observed by TEM and determined by BET, are aggregated in rough particles (170–360 nm) showed with the PCS technique, which gather in micrometric agglomerate, detected by TEM.

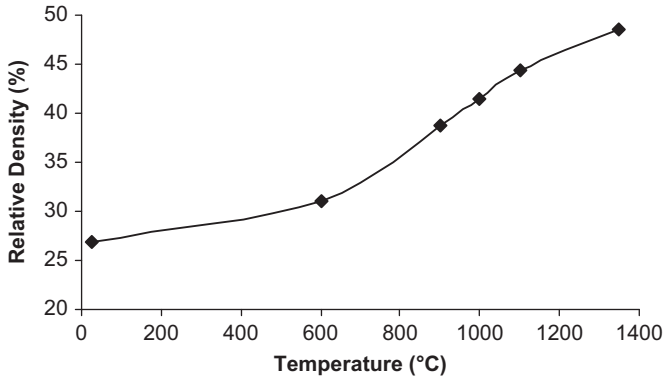

Fig. 7. Relative density of sintered pellets versus temperature.

3.2. Sintering process

In SOFC technology the anodic side realises the contact between hydrogen or hydrocarbon gas and ionic oxygen provides by the electrolyte. This reaction produces water. To enhance the surface exchange between oxygen and fuel and to evacuate water the anodic compound has to be porous (relative density close to 40%). To reach this goal, LSCrRu powder was pressed at 250 MPa into a working mould (20 mm in diameter). Pellets were then sintered at different temperature during 10 h using a heating rate of 2 °C min^{-1}. To prevent LSCrRu decomposition the thermal treatment was realised under Ar atmosphere. Fig. 7 shows the relative density for the sintered pellets versus temperature. To ensure mechanical resistance and presence of porosity the sintering temperature is fixed at 1000 °C. After sintering process the low density rate revealed (42%) is in accordance with the objectives.

The microstructure of the pellet was then observed by scanning electron microscopy (Fig. 8). It confirms the pellets porous state. Broad pores appear with a size superior to the micrometre. Pore enlargement shows a microstructure composed of isotropic LSCrRu grains.

XRD pattern is similar to Fig. 2 and presents a single phase corresponding to $La_{0.75}Sr_{0.25}Cr_{0.93}Ru_{0.07}O_{3-\delta}$. The grain size, estimated using Debye–Scherrer formula's, is close to 200 nm.

All these observations lead to propose a model for the LSCrRu sintering step (Fig. 9). Due to the high surface energy, particles with 10 nm diameter are forming larger particles (200 nm) in the beginning of the sintering process. At high temperature there is particle aggregation in micrometric lump and pore creation between these elements.

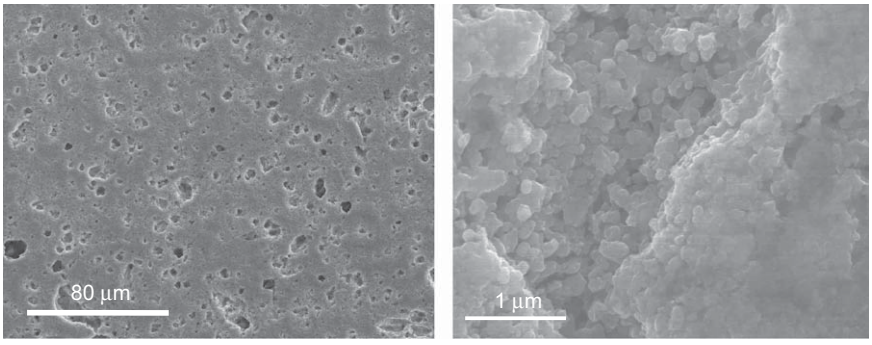

Fig. 8. Fracture surface observation on LSCrRu pellet after sintering at 1000 °C.

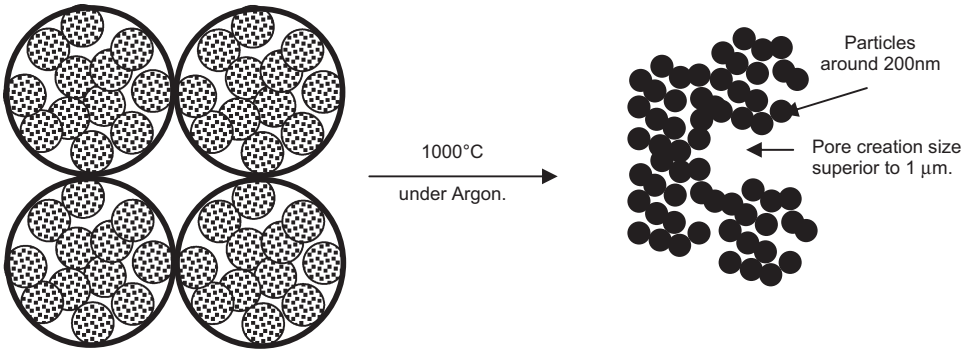

Fig. 9. Sintering model for the LSCrRu microwave synthesised powder.

4. Conclusions

The RAMO system associates advantages solution nucleation processes with microwave heating (core heating and heating rate). This process appears as an efficient source of energy to produce nanoparticles (10 nm diameter) with complex composition as $La_{0.75}Sr_{0.25}Cr_{0.93}Ru_{0.07}O_{3-\delta}$ perovskite materials. Furthermore this technique ensures the Ru integration. The main differences between similar materials produced with other technique are the saving time and a slightly small averaged size.

The surface area value gives well sinterability property and permits to produce porous anode in accordance with the desire application at low temperature (1000 °C). A sintering model for the LSCrRu microwave synthesised powder is proposed to explain pore creation.

References

[1] S. Carter, A. Selcuk, R.J. Chater, J. Kajada, J.A. Kilner, B.C.H. Steele, Solid State Ionics 53 (1992) 605.
[2] C. Sun, U. Stimming, J. Power Sources 171 (2007) 247.
[3] K. Hilpert, R.W. Steinbrech, F. Boroomand, E. Wessel, F. Meshke, A. Zuev, O. Teller, H. Nickel, L. Singheiser, J. Eur. Ceram. Soc. 23 (2003) 3009.
[4] A. Zuev, L. Singheiser, K. Hilpert, Solid State Ionics 147 (2002) 1.
[5] H. Hayashi, M. Watanabe, M. Ohuchida, H. Inaba, Y. Hiei, T. Yamamoto, M. Mori, Solid State Ionics 144 (2001) 301.
[6] M. Mori, T. Yamamoto, H. Itoh, T. Watanabe, J. Mater. Sci. 32 (1997) 2423.
[7] C.F. Khattak, D.E. Cox, Mater. Res. Bull. 12 (1977) 463.
[8] J. Sfeir, P.A. Buffat, P. Möckli, N. Xanthopoulos, R. Vasquez, H.J. Mathieu, J. Van herle, K.R. Thampi, J. Catal. 202 (2001) 229.
[9] T. Hibino, A. Hashimoto, M. Yano, M. Suzuki, M. Sano, Electrochim. Acta 48 (2003) 2531.
[10] T. Caillot, P. Gelin, J. Dailly, G. Gauthier, C. Cayron, J. Laurencin, Catal. Today 128 (2007) 264.
[11] A.L. Sauvet, J. Fouletier, F. Gaillard, M. Primet, J. Catal. 209 (2002) 25.
[12] A.L. Sauvet, J. Fouletier, Electrochim. Acta 47 (2001) 987.
[13] A.L. Sauvet, J.T.S. Irvine, Solid State Ionics 167 (2004) 1.
[14] A.L. Sauvet, J. Fouletier, J. Power Sources 101 (2001) 259.
[15] S. Georges, G. Parrour, M. Henault, J. Fouletier, Solid State Ionics 177 (2006) 2109.
[16] B.D. Madsen, W. Kobsiriphat, Y. Wang, L.D. Marks, S.A. Barnett, J. Power Sources 166 (2007) 64.
[17] S. Barison, M. Battagliarin, S. Daolio, M. Fabrizio, E. Miorin, P.L. Antonucci, S. Candamano, V. Modafferi, E.M. Bauer, C. Bellitto, Solid State Ionics 177 (2007) 3473.
[18] E. Djurado, C. Roux, A. Hammou, J. Eur. Ceram. Soc. 16 (1996) 767.
[19] R. Ran, D. Weng, X. Wu, J. Fan, L. Qing, Catal. Today 126 (2007) 394.
[20] H. Yan, X. Huang, Z. Lu, H. Huang, R. Xue, L. Chen, J. Power Sources 68 (1997) 530.
[21] A. Loupy, Microwaves in Organic Synthesis 2, completely revised and enlarged edition, vol. XXVI, Wiley-VCH, Weinheim, August 2006, 1007pp. 2 volumes, hardcover, Handbook/Reference Book, ISBN-10: 3-527-31452-0, ISBN-13: 978-3-527-31452-2.
[22] D. Stuerga, P. Gaillard, Tetrahedron 52 (1996) 5505.
[23] K. Bellon, P. Rigneau, I. Zahreddine, D. Stuerga, EPJ Appl. Phys. 7 (1999) 41.
[24] L. Combemale, G. Caboche, D. Stuerga, D. Chaumont, Mater. Res. Bull. 40 (2005) 529.
[25] K. Bellon, D. Chaumont, D. Stuerga, J. Mater. Res. 16 (2001) 2619.
[26] E. Gresssel-Michel, D. Chaumont, D. Stuerga, J. Colloid Interface Sci. 285 (2005) 674.
[27] T. Caillot, D. Aymes, D. Stuerga, N. Viart, G. Pourroy, J. Mater. Sci. 37 (2002) 5153.
[28] C. Bousquet-Berthelin, D. Stuerga, J. Mater. Sci. 40 (2005) 253.
[29] J.A.M. van Roosmalen, E.H.P. Cordfunke, Solid State Ionics 52 (1992) 303.
[30] D.R. Lide, CRC Handbook of Chemistry and Physics, CRC Press, New York, 1991.
[31] S. Miyoshi, S. Onuma, A. Kaimai, H. Matsumoto, K. Yashiro, T. Kawada, J. Mizusaki, H. Yokokawa, J. Solid State Chem. 177 (2004) 4112.
[32] D.E. Appleman, H.T. Evan Jr., PB Repr. 216183/3, US Nat. Tech. Serv. Washington, 1973, p. 65.
[33] K.C. Smith, Y.M. Sun, N.R. Mettlach, R.L. Hance, J.M. White, Thin Solid Films 376 (2000) 73.
[34] L. Nougaret, P. Combette, R. Arinero, J. Podlecki, F. Pascal-Delannoy, Thin Solid Films 515 (2007) 3971.